Multifaceted dynamics and gap solitons in $\mathcal{PT}$-symmetric periodic structures

S. Vignesh Raja,[1,*] A. Govindarajan,[2,†] A. Mahalingam,[1,‡] and M. Lakshmanan[2,§]
[1]*Department of Physics, Anna University, Chennai-600 025, India*
[2]*Centre for Nonlinear Dynamics, School of Physics, Bharathidasan University, Tiruchirappalli-620 024, India*

(Received 14 May 2019; published 30 September 2019)

We report the role of $\mathcal{PT}$ symmetry in switching characteristics of a highly nonlinear fiber Bragg grating (FBG) with cubic-quintic-septimal nonlinearities. We demonstrate that the device shows bistable (multistable) states in the broken regime as a direct consequence of the shift in the photonic band gap influenced by both $\mathcal{PT}$ symmetry and higher-order nonlinearities. We also numerically depict that such FBGs provide a productive test bed where the broken $\mathcal{PT}$-symmetric regime can be exploited to set up all-optical applications such as binary switches, multilevel signal processing, and optical computing. Unlike optical bistability (OB) in the traditional and unbroken $\mathcal{PT}$-symmetric FBG, it exhibits many peculiar features such as flat-top stable states and ramplike input-output characteristics before the onset of OB phenomenon in the broken regime. The gain-loss parameter plays a dual role in controlling the switching intensities between the stable states which are facilitated by reversing the direction of light incidence. We also find that the gain-loss parameter tailors the formation of gap solitons pertaining to transmission resonances which clearly indicate that it can be employed to set up optical storage devices. Moreover, the interplay between gain and loss and higher-order nonlinearities brings notable changes in the nonlinear reflection spectra of the system under constant pump powers. The influence of each control parameter on the switching operation is also presented in a nutshell to validate that FBG offers more degrees of freedom in controlling light with light.

DOI: 10.1103/PhysRevA.100.033838

I. INTRODUCTION

In the era of high-speed information exchange, all-optical switches and logic devices are versatile components in all-optical communication systems which have led to widespread research across different devices such as couplers [1,2], Bragg gratings [3], ring resonators [4], and so on. Among these devices, fiber Bragg gratings (FBGs) have engrossed an ever-mounting attention as they afford a larger degree of freedom and flexibility to engineer any spectral characteristics of interest [5] and are potential candidates for provisioning, protection, packet switching, and external modulation applications [6] in addition to sensing, dispersion compensation, and filtering functionalities [7]. Since the bandwidth of the device is very narrow, a small change in refractive index introduced into the system via an external signal is sufficient enough to detune the in-built photonic band gap from its resonance wavelength. Thus, the structure allows light transmission at the wavelengths which were inhibited to transmit previously. This gives the comprehensive picture of the underlying mechanism to realize all these functionalities including optical switching [8].

Optical bistability (OB) is a ubiquitous phenomenon in the framework of nonlinear feedback systems such as Bragg gratings [8], nonlinear Fabry-Pérot cavity [9], ring resonators [10], and even in the case of nonlinear directional couplers with the aid of metamaterials [11,12]. As the name suggests, any nonlinear variation in input intensity results in two or more stable states [optical multistability (OM)] for the given incident intensity. Apart from its conventional application in the form of optical switches or memory devices where the two stable states can be customized as binary logic, researchers have also exploited the possibility to build all-optical transistors, limiters, inverters [13], and signal processing devices [14]. In principle, optical bistability emanates itself as a result of light-dependent refractive index changes or absorption changes inside the structure upon which they are categorized as dispersive or absorptive optical bistability [15]. Ever since the breakthrough work by Winful *et al.* [16], the studies on optical bistability in nonlinear feedback structures primarily focused on understanding the underlying physics behind its operation at various conditions [8,17] which in turn aided the possibility to realize various nonlinear applications [13]. These studies indicate that the bistable curve or the hysteresis loop can be manipulated at will with the aid of any control parameter originating from the device such as device length, detuning parameter, the strength of modulation [3], or via an external control in the form of probe and pump pulse parameters [13]. Some of these factors will be discussed in detail in this paper in later sections.

A suitable choice of materials is an essential ingredient to realize an all-optical switch with low threshold and high figure of merit (FOM) [18,19]. In this regard, optical properties of many nonlinear glasses have been reported in the literature from both theoretical [20] as well as experimental [18,19] perspectives. Particularly, chalcogenide glass that accounts

*vickyneeshraja@gmail.com
†govin.nld@gmail.com
‡drmaha@annauniv.edu
§lakshman.cnld@gmail.com

for both cubic-quintic and septimal nonlinearities has been subjected to intense investigations [18–25]. The nonlinear coefficient of chalcogenide is quite larger than silica and is of the order of 10^3. Thus, it can reduce the threshold level considerably [26]. Yosia *et al.* have reported the formation of nonoverlapping bistable states influenced by a phase-shifted cubic-quintic grating [27]. It is noteworthy to mention that unlike Kerr nonlinearity driven bistability, it offered two completely different approaches to switch into the high state [28]. Recently, Yosefi *et al.* have demonstrated the soliton switching in nonlinear FBG with higher-order nonlinearity [14]. These kinds of studies ensure that higher-order nonlinearities when properly exploited can play a remarkable role in the next-generation signal processing devices.

Having discussed concisely the general aspects of the device, we now wish to stress the importance of $\mathcal{PT}$ symmetry in the current generation optical devices. In the context of optics, the practicality of inherent loss in any functional device was not considered by the scientific community for many years [29]. But, with the advent of parity-time-symmetry ($\mathcal{PT}$) concept, these losses are no longer considered to be detrimental by virtue of the delicate balance between amplification and attenuation [30,31] in the system as in the case of $\mathcal{PT}$-symmetric couplers [32,33], $\mathcal{PT}$ metamaterials [34], $\mathcal{PT}$ microring laser [35], $\mathcal{PT}$ gratings [36,37], $\mathcal{PT}$ laser cavities [38,39], etc. Although this notion traces its origin to the field of quantum mechanics way back in 1998 [40], the translation of the concept on to photonic platform paved the way for its major theoretical advancements [31,41,42] and the first experimental realization by Rütter *et al.* on a $LiNbO_3$ waveguide [43]. $\mathcal{PT}$-symmetric photonics is regarded as the booming field in the last decade or so thanks to some unconventional features possessed by these devices ranging from broadband unidirectional invisibility [41], coherent perfect absorption [39] to coherent amplification [44], controllable bidirectional laser emission [35], and so forth, which are not viable in the perspective of existing systems. Driven by the luxury that refractive index, gain and loss coefficients can be manipulated at ease [31], there is an increasing number of contributions in the literature dedicated to potential applications of $\mathcal{PT}$-symmetric systems, namely, optical isolators, low-power optical diodes [45], signal processing devices [46], single-mode lasing cavities [38], soliton switches [32], and logic devices [46].

To realize a $\mathcal{PT}$-symmetric periodic structure, it is necessary to maintain an equilibrium between generation and annihilation of photons so that it offers no net amplification. In a nutshell, the complex refractive index should satisfy the condition $n(z) = n^*(-z)$. In analogy to its quantum counterpart, optical $\mathcal{PT}$-symmetric media exhibit phase transition at the so-called exceptional point. Hence, the operation of the $\mathcal{PT}$-symmetric grating is stable below a critical amount of gain and loss and when it is violated, the grating exhibits exponential energy growth or lasing behavior [46].

Surprisingly, the inclusion of loss to the traditional structures had an affirmative role in its functionality [29]. For instance, contemporary work by Govindarajan *et al.* on steering dynamics of $\mathcal{PT}$-symmetric coupled waveguides [32] has marked an immense reduction in the power requirement for switching and huge amplification of pulse power. The interplay between nonlinearity and $\mathcal{PT}$ symmetry has impacted in a fall in intensity of the bistable threshold as reported by Phang *et al.* [37,46,47]. They have also reported a switching time of 2.5 ps in one of their works, which hints that these systems are well suited to exploit switching and logic operations [37]. It is worthwhile to mention that $\mathcal{PT}$-symmetric optical devices are undoubtedly far more competent than systems exhibiting no loss or systems with only gain [29]. As of now, the switching characteristics in $\mathcal{PT}$-symmetric fiber Bragg gratings is briefly studied only with conventional silica grating with third-order nonlinearity [48]. Following these works, we here study the role of defocusing quintic nonlinearity combined with self-focusing cubic and septimal nonlinearities on switching of $\mathcal{PT}$-symmetric fiber Bragg gratings. We highlight the role of every individual parameter in dictating the bistable and multistable phenomena in both the unbroken as well as broken $\mathcal{PT}$-symmetric regimes. The study also includes the formation of gap solitons corresponding to the resonance peaks of transmission curves in the presence of higher-order nonlinearities and $\mathcal{PT}$ symmetry. We have also investigated the effects of nonlinearities and $\mathcal{PT}$ symmetry on the spectra of the system in the presence of constant pump power.

The plan of the paper is as follows. Section II describes the necessary mathematical formulation for the system of interest. Sections III and IV give brief explanations of the switching characteristics in the unbroken and broken $\mathcal{PT}$-symmetric regimes, respectively. Section V reveals the gap soliton formation at resonance peaks. Section VI elucidates the switching characteristics of the system in the presence of constant pump power. Finally, in Sec. VII we discuss the significance of the results.

II. THEORETICAL MODEL

We consider a $\mathcal{PT}$-symmetric fiber Bragg grating of period Λ inscribed on the core of a fiber of refractive index n_0 and length L. The nonlinearity of the fiber is not merely restricted to cubic nonlinearity, but it also takes account of the quintic and septimal nonlinearities. The complex refractive index distribution $[n(z)]$ profile that describes such a $\mathcal{PT}$-symmetric system is mathematically written as [49]

$$n(z) = n_0 + n_{1R}\cos\left(\frac{2\pi}{\Lambda}z\right) + in_{1I}\sin\left(\frac{2\pi}{\Lambda}z\right) + n_2|E|^2 + n_4|E|^4 + n_6|E|^6. \quad (1)$$

The strength of modulation parameter is defined by (n_1), which has both real (n_{1R}) and imaginary parts (n_{1I}) and the imaginary term stands for gain $(+n_{1I})$ or loss $(-n_{1I})$ dictated by the so-called $\mathcal{PT}$-symmetric potential, and the last three terms signify self-focusing (n_2, $n_6 > 0$) and self-defocusing ($n_4 < 0$) nonlinearities. The transverse electric field $E(z,t)$ inside the FBG is the superposition of two counterpropagating modulated modes which can be written mathematically as

$$E(z,t) = E_f(z,t)\exp[i(\beta_0 z - \omega_0 t)] + E_b(z,t)\exp[-i(\beta_0 z - \omega_0 t)], \quad (2)$$

where the envelope functions $E_f(z,t)$ and $E_b(z,t)$ that are used to describe the electric fields in the forward and

backward directions obey the slowly varying envelope (paraxial) approximation (SVEA). The propagation constant of the fiber without grating is given by $\beta_0 = 2\pi n_0/\lambda_0$, where λ_0 is the free-space wavelength. The Bragg wavelength of the grating is expressed as $\lambda_b = 2n_0\Lambda$. Practically, the Bragg wavelength is taken in the telecommunication regime, which lies at 1.55 μm. But, it can be chosen anywhere from visible region to infrared by suitably altering the grating period (Λ). Note that the typical values of Λ for a short FBG can vary from 200 to 800 nm.

The coupled mode equations, which describe the light propagation in the proposed system, are given by [27,50]

$$+i\left(\frac{\partial E_f}{\partial z}+\frac{n_0}{c}\frac{\partial E_f}{\partial t}\right)+(k_0+g_0)\exp(-i2\delta_0 z)E_b+\gamma_0(|E_f|^2+2|E_b|^2)E_f-\Gamma_0(|E_f|^4+6|E_f|^2|E_b|^2+3|E_b|^4)E_f$$
$$+\sigma_0(|E_f|^6+12|E_f|^4|E_b|^2+18|E_b|^4|E_f|^2+4|E_b|^6)E_f=0, \tag{3}$$

$$-i\left(\frac{\partial E_b}{\partial z}-\frac{n_0}{c}\frac{\partial E_b}{\partial t}\right)+(k_0-g_0)\exp(+i2\delta_0 z)E_f+\gamma_0(|E_b|^2+2|E_f|^2)E_b-\Gamma_0(|E_b|^4+6|E_f|^2|E_b|^2+3|E_f|^4)E_b$$
$$+\sigma_0(|E_b|^6+12|E_b|^4|E_f|^2+18|E_f|^4|E_b|^2+4|E_f|^6)E_b=0. \tag{4}$$

We adopt the well-known transformation $E_{f,b} = A_{f,b}\ \exp(\mp\delta_0 z)$ and further consider the synchronous approximation (SVEA) to obtain the time-independent equations [16]. Hence, the governing equations for the propagation of continuous waves (CW) become

$$+i\frac{dA_f}{dz}+\delta_0 A_f+(k_0+g_0)A_b+\gamma_0(|A_f|^2+2|A_b|^2)A_f-\Gamma_0(|A_f|^4+6|A_f|^2|A_b|^2+3|A_b|^4)A_f$$
$$+\sigma_0(|A_f|^6+12|A_f|^4|A_b|^2+18|A_b|^4|A_f|^2+4|A_b|^6)A_f=0, \tag{5}$$

$$-i\frac{dA_b}{dz}+\delta_0 A_b+(k_0-g_0)A_b+\gamma_0(|A_b|^2+2|A_f|^2)A_b-\Gamma_0(|A_b|^4+6|A_b|^2|A_f|^2+3|A_f|^4)A_b$$
$$+\sigma_0(|A_b|^6+12|A_b|^4|A_f|^2+18|A_f|^4|A_b|^2+4|A_f|^6)A_b=0. \tag{6}$$

The detuning parameter in the coupled equation is given by $\delta_0 = (2\pi n_0)(\frac{1}{\lambda_o}-\frac{1}{\lambda_b})$. The stop band of the grating is expressed as $|\delta_0| \leqslant k_0$, where k_0 is the strength of coupling between the oppositely traveling fields. Within this band, no propagating modes are supported by the grating and so the light transmission is prohibited [5]. The coefficients of coupling, gain-loss, cubic, quintic, and septimal nonlinearities are given by [27,50]

$$\kappa_0 = \pi n_{1R}/\lambda_0, \quad g_0 = \pi n_{1I}/\lambda_0, \quad \gamma_0 = 2\pi n_2/\lambda_0, \quad \Gamma_0 = 2\pi n_4/\lambda_0, \quad \sigma_0 = 2\pi n_6/\lambda_0. \tag{7}$$

From the fundamentals of $\mathcal{PT}$ symmetry, it is well known that the system is said to be in the unbroken regime if $k_0 > g_0$. On the other hand, if $g_0 > k_0$ the system is set to operate in the broken regime. The condition in which $k_0 = g_0$ is called *singularity* or the *exceptional point.* The following transformation is adapted [49] to obtain normalized coupled mode equations

$$\zeta = \frac{z}{z_0}, \quad u = \frac{A_f}{\sqrt{P(0)}}, \quad v = \frac{A_b}{\sqrt{P(0)}}, \tag{8}$$

where $P(0) = |u_0|^2$ is the intensity of the input laser pulse. The normalized coupled mode equations are given by

$$+i\frac{du}{d\zeta}+\delta u+(k+g)v+\gamma(|u|^2+2|v|^2)u-\Gamma(|u|^4+6|u|^2|v|^2+3|v|^4)u$$
$$+\sigma(|u|^6+12|u|^4|v|^2+18|v|^4|u|^2+4|v|^6)u=0, \tag{9}$$

$$-i\frac{dv}{d\zeta}+\delta v+(k-g)u+\gamma(|v|^2+2|u|^2)v-\Gamma(|v|^4+6|u|^2|v|^2+3|u|^4)v$$
$$+\sigma(|v|^6+12|u|^2|v|^4+18|v|^2|u|^4+4|u|^6)v=0. \tag{10}$$

The normalized parameters are given by

$$\delta = \delta_0 z_0, \quad k = k_0 z_0, \quad g = g_0 z_0,$$
$$\gamma = \gamma_0 P(0) z_0, \quad \Gamma = \Gamma_0 P(0) z_0, \quad \sigma = \sigma_0 P(0) z_0. \tag{11}$$

Further output intensity can be defined as $P_1(L) = |u(L)|^2$. These coupled mode equations (9) and (10) are solved by implicit Runge-Kutta fourth-order method with the following boundary conditions [26]:

$$u(0) = u_0,$$
$$v(L) = 0. \tag{12}$$

Before proceeding to analyze the switching characteristics in detail, we now investigate the role of nonlinearity and the gain-loss coefficient on the photonic band gap of the device.

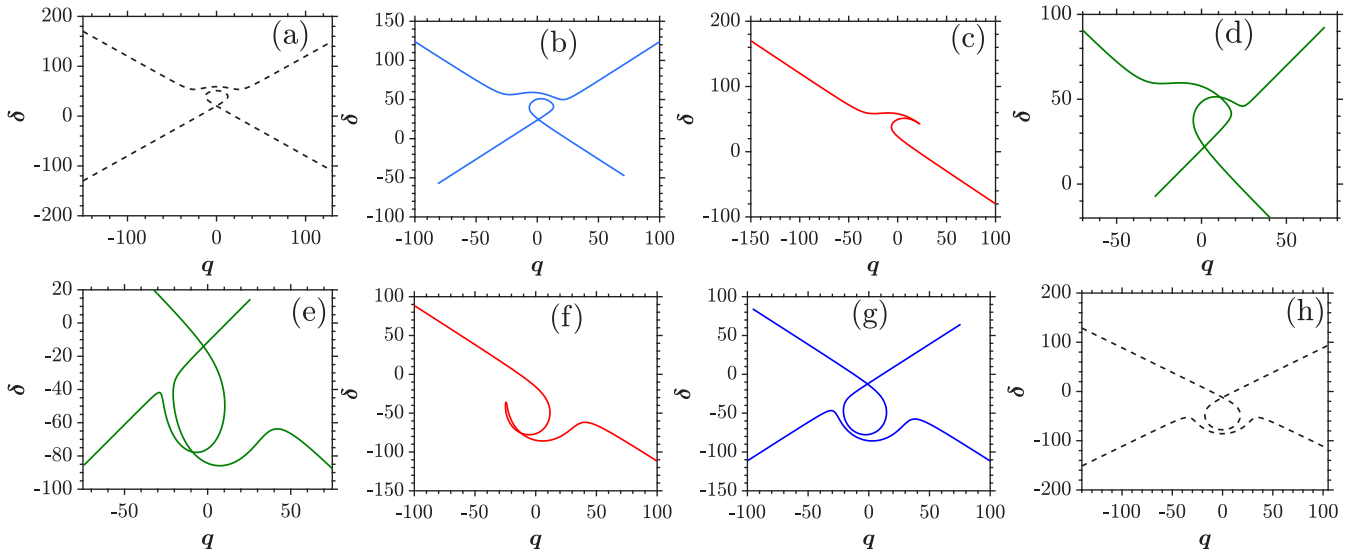

FIG. 1. Nonlinear dispersion curves plotted at $J = 2.5$ for a FBG with $k = 4$. The top panels represent the relation between q and δ in the presence of cubic-quintic nonlinearities ($\gamma = 2$, $\Gamma = 4$, $\sigma = 0$) and the bottom panels correspond to q vs δ curve in the presence of cubic-quintic-septimal nonlinearities ($\gamma = 2$, $\Gamma = 4$, $\sigma = 2$). (a), (h) Illustrate the existence of photonic band gap in the absence of $\mathcal{PT}$ symmetry. (b), (g) Depict the narrowing of band gap in the unbroken $\mathcal{PT}$-symmetric regime ($g = 2$). (c), (f) Plotted at the exceptional point ($g = 4$). (d), (e) Show the dispersion curves in the broken $\mathcal{PT}$-symmetric regime ($g = 5$).

The existence of such a gap is a typical characteristic of any feedback structure and it is already discussed in the context of conventional FBG and $\mathcal{PT}$-symmetric cubic FBG in the literature [21,49,50]. The mathematical expressions for the dispersion relation of a highly nonlinear $\mathcal{PT}$-symmetric FBG can be found by substituting the continuous wave solution into the normalized coupled equations given by (9) and (10). The wave solutions represent u and v in terms of forward and backward wave amplitudes $\psi_{1,2}$ along the length of propagation of the incident field inside the grating and they are given by

$$u = \psi_1 \exp^{iq\zeta}, \quad v = \psi_2 \exp^{iq\zeta}. \tag{13}$$

Here, ψ_1 and ψ_2 are assumed to be real constants. The ratio of ψ_2/ψ_1 is assumed as a new parameter f. The sum of ψ_1^2 and ψ_2^2 gives the total power (J) of the propagating wave. The relation between $\psi_{1,2}$ and J is written as

$$\psi_1 = \sqrt{\frac{J}{1+f^2}}, \quad \psi_2 = \sqrt{\frac{J}{1+f^2}}\, f. \tag{14}$$

Hence, one obtains the nonlinear dispersion relation between q and δ by using Eqs. (13) and (14) in (9) and (10) as

$$q = -\frac{k}{2f}(1-f^2) + \frac{g}{2f}(1+f^2) - \frac{\gamma J}{2}\left(\frac{1-f^2}{1+f^2}\right) + \Gamma J^2\left(\frac{1-f^2}{1+f^2}\right) - \frac{3\sigma J^3}{2}\left(\frac{1-f^6+2f^2-2f^4}{(1+f^2)^3}\right), \tag{15}$$

$$\delta = -\frac{k}{2f}(1+f^2) + \frac{g}{2f}(1-f^2) - \frac{3\gamma J}{2} + 2\Gamma J^2\left(1+\frac{f^2}{(1+f^2)^2}\right) - \frac{5\sigma J^3}{2}\left(1+\frac{3f^2}{(1+f^2)^2}\right). \tag{16}$$

From Figs. 1(a)–1(h), one can visualize two branches in the dispersion curve admitted by Eqs. (15) and (16). These two branches correspond to the normal dispersion regime ($f > 0$) and the anomalous dispersion regime ($f < 0$). It should be noted that the dispersion curve pertaining to linear and cubic nonlinearity has already been discussed in Refs. [49,50] and so we here focus only on quintic and septimal nonlinearities. In the presence of quintic nonlinearity, a loop is formed at the lower branch of the q vs δ curve. Any increase in the value of Γ increases the size of the loop and vice versa. The loop disappears at lower values of Γ as a result of perfect balance between self-focusing cubic nonlinearity and self-defocusing quintic nonlinearity. In the unbroken $\mathcal{PT}$ regime, with increase in g, the shape remains the same as in the case of conventional FBG [cf. Figs. 1(a) and 1(b)]. As we increase the value of g, the loop in the lower branch is shifted toward higher value of q as shown in Fig. 1(b). At the exceptional point ($g = k$), the band gap vanishes and the formation of loop in the lower branch still persists. Hence, one can control the formation of loop in the dispersion curves by dictating the strength of the nonlinearity. In the broken $\mathcal{PT}$-symmetric regime, we get two curves on the left and right of the center wavelength instead of distinguishable curves on the upper and lower branches [50,51]. The two curves merge and form a closed dispersion curve as seen in Fig. 1(d). The overlap region grows as the value of Γ gets higher. In other words, instead of forming a loop in the lower branch, the intersection of two curves occurs at the center and it expands with increase in the value of Γ in the $\mathcal{PT}$-symmetric broken regime.

In the presence of septimal nonlinearity, a loop is formed at the upper branch of the curve in contrast to the quintic nonlinearity case as seen in Fig. 1(h). Also, the entire dispersion curve is shifted toward lower values of δ. This is because of the additional focusing effect introduced by the septimal nonlinearity. Thus, the formation of loops in the upper or

lower branch is decided by the nature of nonlinearity whether it is self-focusing or self-defocusing, respectively, even in the presence of $\mathcal{PT}$ symmetry. Similar to the previous case, any increase in the value of septimal nonlinearity increases the size of the loop in the upper branch. Likewise, any increase in the value of g in the unbroken $\mathcal{PT}$-symmetric regime shifts the loop toward lower value of q as observed in Fig. 1(g). The plot in Fig. 1(f) also confirms that, at the exceptional point, the band gap closes in the septimal nonlinear regime quite similar to the quintic case, with the difference is being that the loop is now formed in the upper branch. The variations illustrated in Fig. 1(d) hold true for Fig. 1(e) also, except the shift in the curves toward negative values of δ and the increase in the area of the intersection between the two curves. It is worthwhile to mention that all these variations occurring in the photonic band gap of the device are the direct consequence of change in refractive index of the medium induced by interplay between $\mathcal{PT}$-symmetric potential and higher-order nonlinearities. Having elucidated the necessary mathematical description of the system, we now look into the switching characteristics of the proposed system.

III. TRANSMISSION PROPERTIES IN UNBROKEN $\mathcal{PT}$-SYMMETRIC REGIME

The switching characteristics of the $\mathcal{PT}$-symmetric FBG has been investigated in the recent work by Liu *et al.* which reveals that with an increase in gain and loss coefficient, the threshold of switching gets higher [48]. Even though this outcome is an undesired one, additional degrees of freedom offered by the inclusion of $\mathcal{PT}$ symmetry should not be taken lightly. The additional features of $\mathcal{PT}$ symmetry need to be retained but not at the cost of the threshold. On the other hand, we find that the inclusion of higher-order nonlinearities in the conventional FBG aids in the reduction of the threshold. This is the factor that drove us to study the switching characteristics of a highly nonlinear FBG under $\mathcal{PT}$-symmetric notion. Before we proceed to study the individual effects in detail, we portray the combined effects of $\mathcal{PT}$ symmetry with cubic-quintic-septimal nonlinearities on the switching threshold. To do so, numerical simulations were carried out with device parameters $L = 1, k = 3, g = 1.5$, and $\delta = 0$ [41]. The switch-up intensities of cubic, quintic, and septimal nonlinearities were found to be descending in the order 2.6, 1.77, 1.13 [see Fig. 2(b)] and the corresponding values of switch-down intensities are 1.09, 0.49, 0.32, respectively. Such a dramatic decrease in the switch-up intensity and the threshold is provided by the inclusion of higher-order nonlinearities alongside the $\mathcal{PT}$ symmetry. Thus, our system can uniquely combine the pros of the individual systems without imposing any impairments.

A. Effect of length and coupling coefficient

To understand the role of length of the fiber grating and the strength of coupling coefficient, we first consider a simple case in which only the cubic nonlinearity is present ($\Gamma = \sigma = 0$). Figure 3(a) shows the input-output characteristics at $g = 1.5$, $k = 3$, $\delta = 0$ for three different values of the device length $L = 1$, 1.25, and 1.5. When the length is shorter

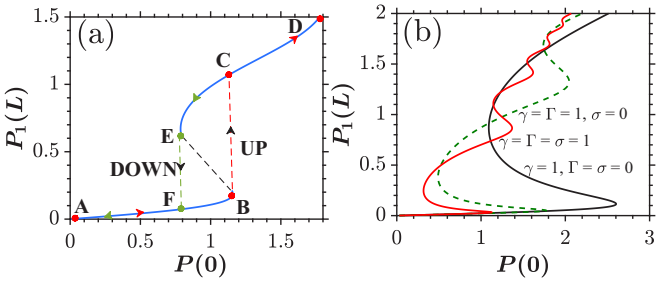

FIG. 2. (a) Schematic sketch showing different branches of a typical bistable curve with their switch-up (marked as B) and switch-down intensities (marked as E). Here, the two stable states are indicated by curves AB and DE and the unstable branch is indicated by BE. (b) Comparison of optical bistable (multistable) characteristics of the unbroken $\mathcal{PT}$-symmetric FBG device under different nonlinear regimes for $L = 1, k = 3, g = 1.5$, and $\delta = 0$.

($L = 1$), the effective feedback to the system gets reduced and therefore we observe only two stable states in the output with a switch-up intensity of 2.603 for $L = 1$. Below this length, the feedback is not sufficient to observe bistability when $k = 3$. The switch-up intensity between the three curves featured a slim difference but an increase in L severely influences the hysteresis width. The differences between the switch-up and switch-down intensities for the three different lengths are 1.51, 1.99, 2.28 (approximately). The upper stable branch gets flatter at higher values of length. The strength of the coupling also influences the shape and width of the hysteresis curve. At the given length ($L = 1$), the lower values of k result in insufficient feedback to create a bistable state. In the simulations, we fix $L = 1$, $g = 1.5$, $\delta = 0$ and for three different values of k the bistability curves are plotted in Fig. 3(b). When $k = 2.5$, the switch-up intensity increases to 2.12 and further it goes to 2.603 at $k = 3$. From this, it is very clear that k not only intensifies the switch-up intensity value but it has a combined influence alongside the device length in increasing the feedback to the system. Hereafter, throughout this paper, the length and the strength of the coupling are fixed at $L = 2, k = 4$ as it is practically feasible to tune the values of gain and loss coefficient and the detuning parameter with an external control rather than the device length and the inherent coupling coefficient. Note that in view of practical realization, the value of coupling parameter k (which can be in the range of 1 to 10 cm^{-1}) goes hand in hand with the length of the

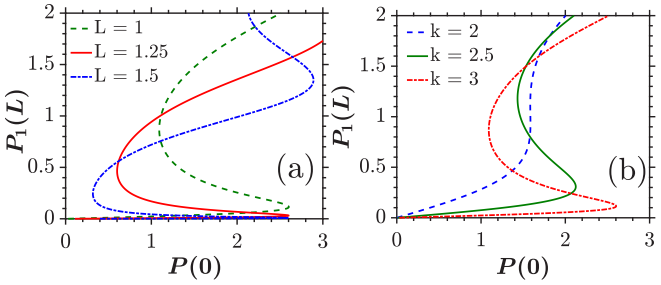

FIG. 3. Role of (a) device length, and (b) the strength of coupling coefficient in the optical bistability phenomenon of an unbroken $\mathcal{PT}$-symmetric FBG.

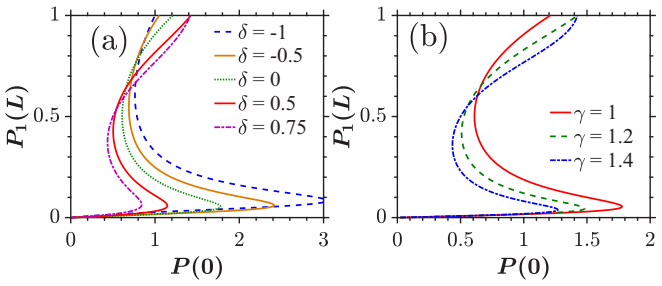

FIG. 4. Output intensity $P_1(L)$ as a function of input intensity $P(0)$ in the unbroken $\mathcal{PT}$-symmetric cubic regime ($\Gamma = \sigma = 0$) of the FBG at fixed values of $g = 3.75$. (a) Plotted for five different values of detuning parameter at $\gamma = 1$. (b) Simulated for three different values of cubic nonlinear coefficient at $\delta = 0$.

grating varying from 1 mm to 10 cm and the optimum value of kL can attain the values from 1 to 10 [52].

B. Role of Kerr (cubic) nonlinearity and detuning parameter

With a clear-cut idea on the role of length and strength of the coupling obtained from the previous section, we directly proceed to study the effect of cubic nonlinearity at a given value of gain and loss coefficient and other device constraints. The importance of the detuning parameter (δ) on the bistable phenomenon is pointed out graphically in Fig. 4(a). If the signal wavelength is away from the Bragg wavelength, it is said to be detuned and depending on whether it is longer or shorter than the Bragg wavelength, it is designated as negative or positive detuning, respectively. Compared to the operation at the synchronized wavelength (refer the plot when $\delta = 0$), detuning in the shorter wavelength reduces the threshold and width of the hysteresis whereas the negative detuning increases the threshold and width of the hysteresis. The switch-up intensities for different values of $\delta = -1$, -0.5, 0, 0.5, and 0.75 at $g = 3.75$ are given by 3.041, 2.413, 1.777, 1.145, and 0.8422, respectively. The series of values in descending order representing the switching intensities look deceiving that one may intend to reduce the threshold by increasing the detuning further. But, this will detune the system outside the band edges and hence results in insufficient feedback to create any bistable feature.

The nonlinear parameter of the fiber purely depends on the concentration of the dopant added to the intrinsic one. Hence, we can have a variety of silica fibers possessing different values of third-order nonlinearity. To elucidate the role of nonlinearity numerically, we set the parameters as $g = 3.75$ and $\delta = 0$ and vary γ from 1 in steps of 0.2. As expected, the higher the value of nonlinearity, the lesser the intensity required to switch between the stable states. In Fig. 4(b), the corresponding values of switch-up intensity for $\gamma = 1$, 1.2, 1.4 are measured as 1.777, 1.481, and 1.269, respectively. Their corresponding switch-down intensities are found to be 0.612, 0.509, and 0.436.

C. Combined effects of cubic-quintic nonlinearities

To illustrate the effect of cubic-quintic nonlinearity on the switching, we set $g = 2$, $\delta = 0$, and $\gamma = 1$ [see Fig. 5(a)].

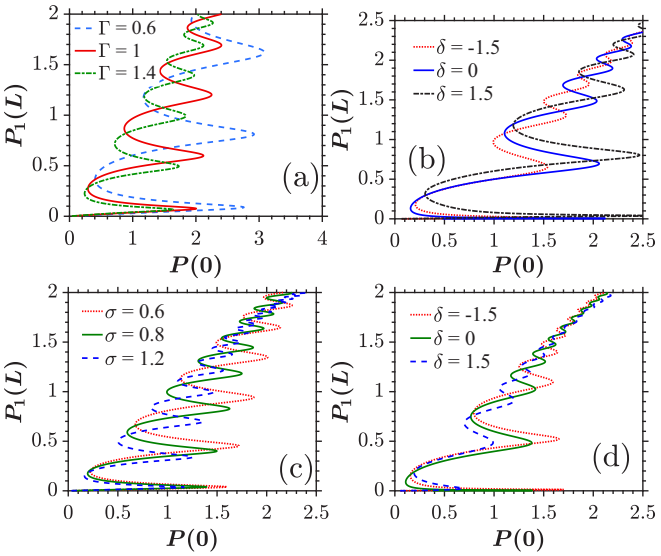

FIG. 5. Illustrations of the variations in the output intensity $P_1(L)$ against input intensity $P(0)$ of an unbroken $\mathcal{PT}$-symmetric FBG. The top panels correspond to the cubic-quintic nonlinear regime $\gamma = \Gamma = 1$, $\sigma = 0$, while the lower panel features FBG with cubic-quintic-septimal nonlinearities ($\gamma = \Gamma = \sigma = 1$). (a), (b) Show the variation with respect to Γ and δ, respectively. The bottom panels represent the same for the septimal case. The figures on the left and right are plotted at $g = 2$ and 3.5, respectively.

When $\Gamma = 0.6$, the switch-up intensity is very high at 2.76 and the hysteresis width is quite large. When Γ is increased to unity, the intensity reduces to 2 with a slim reduction in switch-down intensity from 0.41 to 0.29. The other key difference between the two curves is that, at $\Gamma = 1$, there are more stable branches than at $\Gamma = 0.6$. The switching intensities between the adjacent stable branches also get reduced. More stable states are visible in Fig. 5(a) when Γ is increased to 1.4. The reduction in the switch-up intensity, as well as hysteresis width, is analogous to the cubic nonlinearity case and so the thumb rule to reduce the switch-up intensity is straightforward to pronounce, that is, choose a material with higher nonlinearity regardless of the regime in which it is operated. But, the detuning has a dissimilar influence on switch-up intensity compared to the cubic effect. In the presence of cubic nonlinearity alone, the intensity falls off in the positive detuning regime whereas in the presence of an additional defocusing (quintic) nonlinearity, the intensity decreases when operated in the negative detuning regime as seen from Fig. 5(b). The values of switch-up intensities between second and third stable states for $\delta = 1.5$, 0, -1.5 are 2.45, 2.059, and 1.539, respectively. These values are measured at $g = 3.5$ and $\gamma = \Gamma = 1$. Interpretation of these outcomes implies that when we include the higher-order nonlinearities to the system without imposing any changes to the other parameters, multistable states are observed in its input-output characteristics. These multistable states can be employed in n-level pulse amplitude modulation (PAM) scheme to improve the quality of reconstructed signal provided that the intensity of the regenerated signal is stationed in one of these stable states [53]. Compared to binary modulation scheme,

PAM-4 offers two times larger transmission capacity. Hence, FBG with higher-order nonlinearities in the $\mathcal{PT}$-symmetric unbroken regime can be used in the all-optical short-haul communication networks.

D. Effect of cubic-quintic-septimal nonlinearities

The number of stable states and the threshold of switching in our system can be controlled with ease by carefully adjusting the system parameters. Theoretically, higher-order (2^n) modulation schemes ($n > 3$) can further improve the transmission capacity in short-haul communication network. If such schemes are commercially feasible in the near future, then chalcogenide-based FBG with septimal nonlinearity can play a key role to setup n-PAM signal regenerators since it admits more number of stable states. The thumb rule stated in the previous section holds good even in the presence of septimal nonlinearity, i.e., the higher the septimal nonlinear coefficient, the lower the switch-up intensity required for switching and the width of the hysteresis also decreases with increase in σ as shown in Fig. 5(c). The switch-up powers between the first stable branch and the second branch for three different values of $\sigma = 0.6$, 0.8, and 1.2 are measured as 1.598, 1.393, and 1.167, respectively. The increase in the number of stable branches at larger nonlinear coefficients is also similar to the cubic-quintic case. There is no big difference between the switch-down power between the first and second branches when σ is varied. But, the difference keeps mounting for the succeeding branches on the top of the first bistable curve at higher values of σ as evident from Fig. 5(c). In Fig. 5(d) the switch-up intensity at $\delta = 0$ is measured as 1.384. Since the septimal nonlinearity is a focusing effect, operating the device in the positive detuning regime decreases the switch-up intensity (0.6848 at $\delta = 1.5$), whereas in the negative detuning regime the switch-up intensity is increased (1.7 at $\delta = -1.5$). So, we conclude that the role of detuning in power reduction merely depends on the nature of the higher-order nonlinearities whether it is self-focusing or -defocusing.

E. Role of gain-loss parameter on various nonlinearities

It has been reported that any increase in the value of gain and loss coefficient (g) increases the intensity levels required to switch between the stable states in the presence of cubic nonlinearity [41,48,51]. But, this is true only for a certain range of g values. For the values of g, closer to the value of k it results in the decrease of the switching intensities as in Fig. 6(a). Next, we look into the effect of g in the presence of higher-order nonlinearities. When g is increased gradually in the presence of quintic nonlinearities without violating the unbroken $\mathcal{PT}$-symmetric conditions, the switch-up intensity builds up to 2.058 ($g = 2.25$) via 1.933 ($g = 1.75$), and 1.702 ($g = 1$) as seen in Fig. 6(b). It does not return to the lower branch at the same intensity when the input intensity is decreased. It sustains in the same branch until the input intensity is reduced below 0.332, 0.26, and 0.19, respectively, for the above-mentioned values of g. There is a marginal decrease in the switch-up intensity between the first and second stable branches in the above-mentioned values.

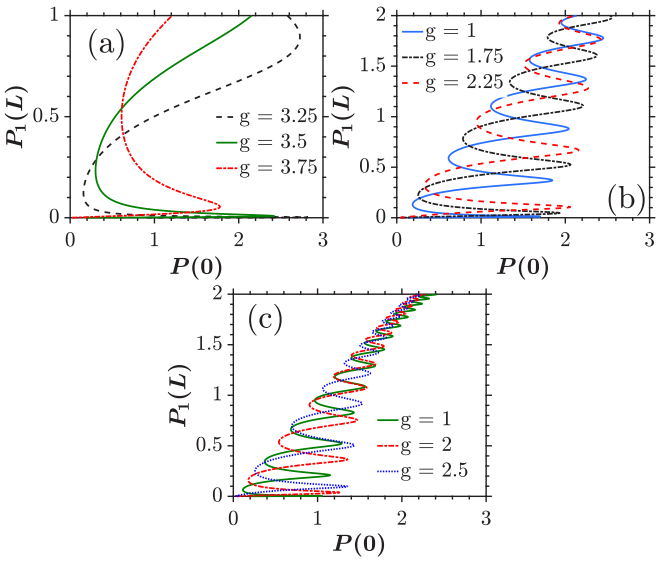

FIG. 6. Plot of the variation in the input-output characteristics of the unbroken $\mathcal{PT}$-symmetric FBG at different values of g with $\delta = 0$ for the left light incidence. The variations are plotted in the presence of (a) cubic nonlinearity alone ($\gamma = 1, \Gamma = \sigma = 0$), (b) cubic-quintic nonlinearities ($\gamma = \Gamma = 1, \sigma = 0$), and (c) combination of cubic-quintic-septimal nonlinearities ($\gamma = \Gamma = \sigma = 1$).

Figure 6(c) exemplifies the role of gain-loss parameter on the system that incorporates all the higher-order nonlinearities ($\gamma = \Gamma = \sigma = 1$) at the Bragg wavelength for three different values of $g = 1$, 2, and 2.25. The switch-up intensity starts to ascend in the order 1.087, 1.261, and 1.435 and the corresponding values of switch-down intensities are measured to be 0.1154, 0.1776, and 0.26. It is very obvious from these studies in the unbroken regime that the desired bistable or multistable curves can be manipulated at ease by judiciously adjusting the imaginary part of the complex refractive index.

The phase-shifted gratings are well known for exhibiting low-intensity switching behaviors compared to other grating structures [8,54]. The $\mathcal{PT}$-symmetric FBGs can exhibit such a low-intensity switching if the direction of incidence of the input pulse is reversed which is not at all feasible in a conventional FBG since it exhibits the same bistable and multistable behaviors in both directions. Thus, the switching phenomenon in a $\mathcal{PT}$-symmetric FBG can be termed as nonreciprocal switching in the sense that it can have an entirely different switching dynamics for left and right incidences.

It is noteworthy to mention at this juncture that the parameter g has a dual role in controlling the switching intensities of the system. By dual role we mean that the device exhibits distinguishable OB and OM curves for the same value of g and other system parameters except for left and right light incidence directions. For instance, there is a weak bistable curve formation at $g = 3.75$ in Fig. 7(a) for the right incidence. Moreover, the switching intensities decrease with an increase in g for the right incidence in contrast to the left light incidence. This sort of dual nature of parameter g on the switching intensities persists even in the presence of quintic nonlinearity as shown in Fig. 7(b) and we can observe more than two stable states for input powers less than unity. Such a

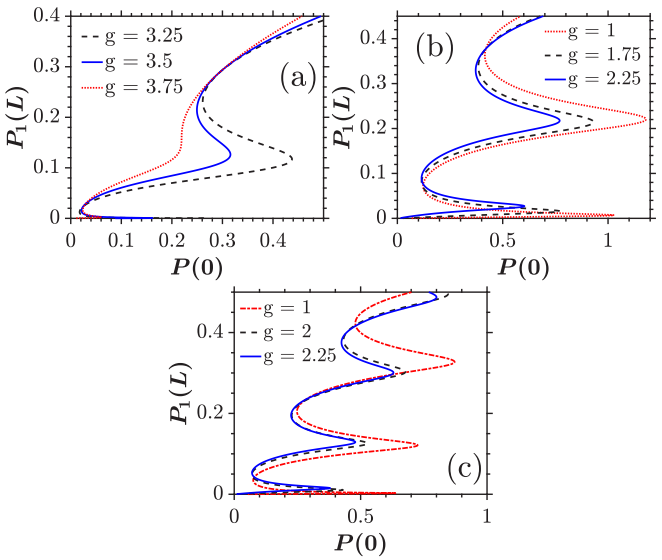

FIG. 7. Plots illustrating the same dynamics with the same system parameter as in Fig. 6 when the light is launched from the right input surface of the FBG.

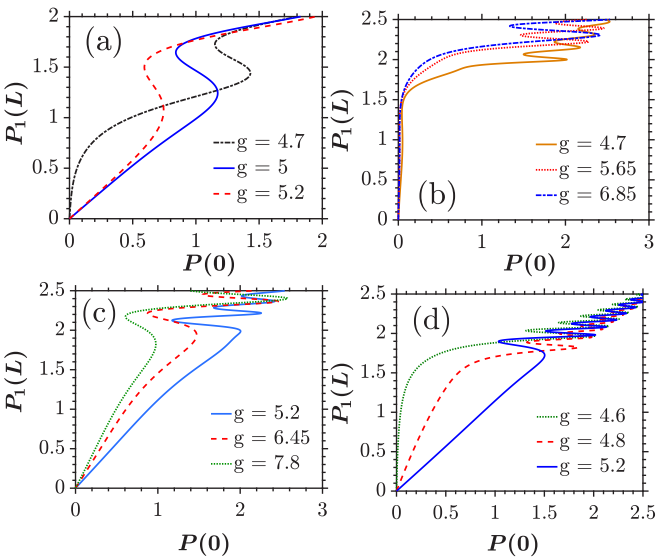

FIG. 8. Plots depicting the optical bistability in a broken $\mathcal{PT}$-symmetric FBG for different values of g at $\delta = 0$ for left incidence. Here, the output and the input intensities of the system are represented by the variables $P_1(L)$ and $P(0)$, respectively. (a) Simulated in the presence of cubic nonlinearity alone ($\gamma = 1$, $\Gamma = \sigma = 0$). (b), (c) Represent the role of g in the presence of cubic-quintic nonlinearities ($\gamma = \Gamma = 1$, $\sigma = 0$). (d) Plotted in the presence of cubic-quintic-septimal nonlinearities ($\gamma = \Gamma = 1$, $\sigma = 0.6$), respectively.

formation of low-power multistable states was not observed in Fig. 6(a). This kind of inverse relationship between the parameter g and the switching intensities and the formation of multistable states at low value of input intensities lasts even with the addition of septimal nonlinearity to the system as seen in Fig. 7(b). The reason for such a behavior is apparent from the fact that the increase in g suppresses the absorption of the forward field intensity for right incidence and vice versa.

IV. BROKEN $\mathcal{PT}$-SYMMETRIC REGIME

A. Influence of gain-loss parameter

We recently became aware of a work which claims that the OB-OM curves cannot occur in the broken $\mathcal{PT}$-symmetric regime [51]. Nevertheless, it has been recently revealed that the broken $\mathcal{PT}$-symmetric regime supports an alternative type of gap solitons which was further termed as dark-gap solitons along with exhibiting an alternative type of optical bistability [55]. Hence, to analyze the issue further, we look at the switching characteristics of the $\mathcal{PT}$-symmetric FBGs with higher-order nonlinearities for the left light incidence. To demonstrate the role of g in the broken regime, the detuning parameter is fixed at $\delta = 0$ and in the first case we neglect the higher-order nonlinearities for the sake of simplicity so that only the cubic nonlinearity has a significant role. When $g = 5.2$ and $\gamma = 1.5$, the system admits a desirable bistable curve with the switch-up intensity around 0.7443 and the corresponding switch-down intensity is measured to be 0.5924 [see Fig. 8(a)]. If the value of g is reduced with no changes to the other settings, a significant amount of increase in the switch-up intensity is observed. In the broken (cubic) $\mathcal{PT}$-symmetric regime, if the value of g is far from the singularity condition, the gain of the system is enhanced rather than absorption within the medium and it must be stressed that this is the much anticipated outcome in the context of any $\mathcal{PT}$-symmetric optical system. Also, from Fig. 8(a), we observe that the value of gain and loss coefficient plays a vital role in deciding the range of intensities over which output state should remain either in the upper branch or the lower branch of the bistability curve. When g is closer to k ($g = 4.7$), the output state remains in the lower branch for a larger range of input intensity. However, if the gain and loss coefficient value is far away from k ($g = 5.2$), it switches to the upper stable state at relatively lower intensities. With a further reduction in the value of gain-loss parameter (g), the system admits multistability at the same input power. This gives an overview of the optimum choice of g parameter to get the desired bistability or multistability.

We further portray the effect of variation of parameter g when the quintic nonlinearity is added to the system. Unlike the previous case, the system exhibits more than two stable states even at higher values of gain and loss coefficient. A decrease in g at a given set of values of nonlinearities $\gamma = 1$ and $\Gamma = 1$ brings about notable changes in the switch-up and switch-down power levels. The number of stable states in the input-output characteristics of the device decreases with an increase in the value of g. Thus, g serves as an additional degree of freedom to control the number of stable states for a given set of device parameters. A phenomenal outcome of the system is that it admits a ramplike first stable output state for certain values of g as seen in Fig. 8(b). This is yet another critical outcome of our investigation. These kinds of ramplike bistable states are already observed in plasmon resonance structures [56,57], graphene-based structures [58,59], silicon waveguide resonators [60], and plexcitonic systems [61]. But, such a OB-OM is observed in a $\mathcal{PT}$-symmetric FBG device, thanks to the judicious balance between the gain and loss.

Analyzing Fig. 8(b) further, one can observe that the range of input intensities over which this ramp behavior is observed decreases when g is reduced. When operated at $g = 4.7$, 5.65, and 6.85 the system concedes a steplike response after a sharp transition from its initial value [see Fig. 8(c)]. It is important to note that such a mix of stable states resembling a ramp and step has previously been observed in a complex nanodimer with a semiconductor quantum dot [61]. These kinds of bistable states with flat slopes can be explored in the construction of signal regenerators [3]. Also, the difference between the two power levels keeps mounting with increase in g which inherently means that the value of g plays a central role in dictating the width of the hysteresis loop. This implies that the same device can be exploited for building applications like switching with low hysteresis width or all optical memories with larger widths, simply by tuning the value of g which is very much feasible compared to other device parameters. The effect of g on the switch-up and switch-down powers persists even at higher values of quintic nonlinearity but the only difference being the increase in the number of stable states as an effect of dominant self-defocusing nonlinearity over the focusing one.

We next consider a condition where all the nonlinearities are taken into account ($\gamma = \Gamma = 1$, $\sigma = 0.6$) and g is varied to find its impact on the switching operation. Similar to the previous case, the system exhibits multiple stable branches for any value of g in this regime. One can easily visualize that the g parameter has a central role in deciding the intensity at which the system switches between the first stable state and the second one shown in Fig. 8(d). At higher values of gain-loss parameter ($g = 5.2$), the second stable state is preceded by a ramplike stable state. On the other hand, if the value of g is fixed at 4.6 and the intensity is tuned from zero, there is a sharp increase in the output intensity from zero to an intensity slightly greater than unity. Following the sharp transmission, the output intensity is steady over a large range of input intensities. In the plot we observe that multiple stable branches start to emanate at higher intensities. The width of each stable branch is lower than the previous one and the first stable branch is characterized by larger hysteresis width. The bistability plots in this regime thus give a conclusive evidence that the value of the switching intensity is inversely proportional to the value of g. It is clear that at two different sets of values of g, there is a drastic change in the behavior of the system which confirms the fact that the system is quite sensitive to smaller variations of gain and loss.

It is noteworthy to mention that the low-intensity switching phenomenon for the right incidence can happen even in the broken $\mathcal{PT}$-symmetric regime. To do so, we simulate the system with the same set of parameters as in Fig. 8 for the right incidence. The hysteresis curve in Fig. 9(a) looks more or similar to the one that we observed in Fig. 8(a). Nevertheless, the OB phenomenon is observed at very low input intensities. The switch-up intensities for different values of $g = 4.7$, 5, and 5.2 are measured to be 0.23, 0.152, and 0.08, respectively. With the addition of quintic nonlinearity into the system, the device can exhibit both ramplike and steplike first stable states [see Figs. 9(b) and 9(c)], resembling the curves obtained in Figs. 8(b) and 8(c), respectively. For $P_0 < 1$, there is no formation of multistable states as seen in Figs. 8(b) and 8(c),

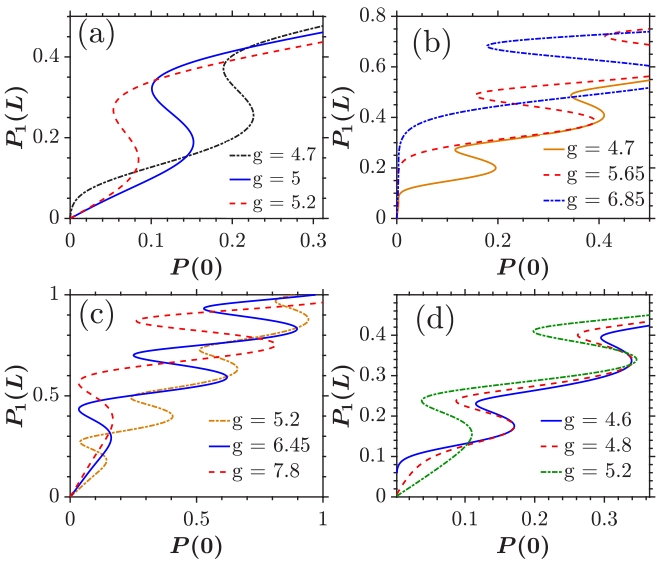

FIG. 9. Plots depicting the same dynamics with the same system parameters as in Fig. 8 for the right light incidence.

whereas we obtain multiple stable states with very low switching intensities in Figs. 9(b) and 9(c) for the same value of P_0. The same explanation holds good with the inclusion of septimal nonlinearity too as observed in Fig. 9(d). The study of OB-OM curves in the broken $\mathcal{PT}$-symmetric regime for the right incidence thus opens a new avenue for fabricating all-optical switches and memory devices which require ultralow switching intensities with different launching conditions.

B. Effect of variation of detuning parameter

In the previous sections, the effect of variation of parameter g under various nonlinear regimes and the effect of nonlinearity at fixed g were examined by setting the detuning parameter value to zero which implies that the signal wavelength must be synchronized with the Bragg wavelength. But, there is a strong correlation between the switching intensities (both up and down) and finite detuning values [3,8]. To illustrate the effect of detuning parameter, the value of g is fixed at $g = 5$. Similar to the last section, first we study the effect of detuning in the absence of higher-order nonlinearities. If the device is operated at $\delta = -0.25$, we get a wide bistable curve with switch-up power of 1.371 and switch-down power of 0.9397 and if the same system is operated at $\delta = 0$ the switch-up intensity reduces to 1.173 as seen in Fig. 10(a). This confirms that operating in the negative detuning regime increases the hysteresis width as well as the intensity required to switch between the two stable states. If one intends to reduce the threshold, the device should be operated closer to the band gap or in the positive detuning regime. For instance, if the detuning value is assigned to be $\delta = 0.25$, the intensity to switch between first stable state and second stable state reduces to 0.9741. This intensity value further reduces to 0.7939 for $\delta = 0.5$ with a simultaneous reduction in the hysteresis width. Thus, negative detuning regime favors the device's preference to remain in the first stable branch for a larger range of input intensities, whereas the positive detuning

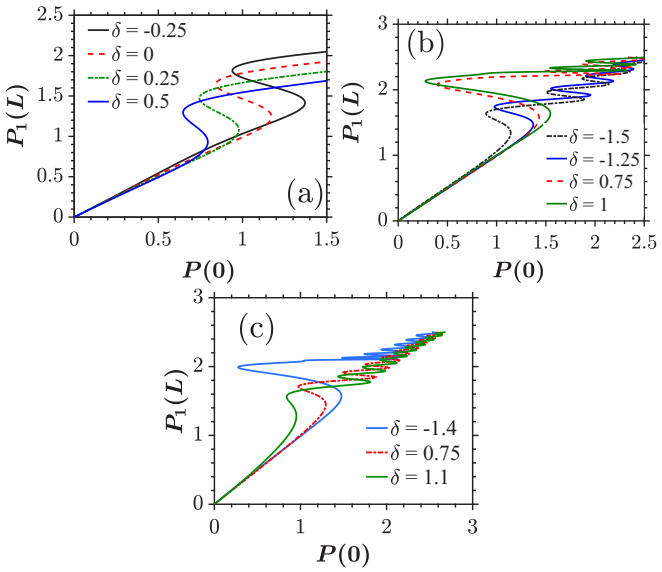

FIG. 10. Effect of varying the detuning parameter δ on the input-output characteristics of a broken $\mathcal{PT}$-symmetric FBG at $g = 5$. Here, the output and input powers are represented by $P_1(L)$ and $P(0)$, respectively. (a) Plotted in the presence of cubic nonlinearity alone ($\gamma = 1.5$, $\Gamma = \sigma = 0$). (b) Represents the simulated results in the presence of cubic-quintic nonlinearities ($\gamma = \Gamma = 1, \sigma = 0$). (c) Plotted in the presence of cubic-quintic-septimal nonlinearities ($\gamma = \Gamma = 1, \sigma = 0.6$).

tends to keep the output intensity in the upper stable branch for a larger range of input intensities.

To portray the effect of detuning in the presence of both cubic and quintic nonlinearities, we set $\gamma = \Gamma = 1$ and $g = 5$. The positive detuning parameter increases the hysteresis width and reduces the number of stable states in the presence of quintic nonlinearity. The plots depicted in Fig. 10(b) give a conclusive evidence that an increase in positive detuning inflates the difference between switch-up and -down intensities which implies that the intensity inside the device is sufficient enough to keep the output state dormant post the switching from its previous state. Hence, it is preferable to use this kind of multistable state in the construction of optical memories rather than switches. If we look at the same system working in the negative detuning regime, the switch-up intensity (between the first two stable states) keeps on deflating and, therefore, if one intends to construct switches with a cubic-quintic FBG in the broken regime, it is preferable to have signal wavelength longer than the Bragg wavelength provided that it lies within the stop band. Also, the number of stable states increases if the device is operated in the negative detuning regime whereas it decreases when operated in the positive detuning regime. Physically, the memory operation can be accomplished by varying the holding-beam input power [62]. As the input intensity varies, the output intensity can stay in one of the stable branches and not in the unstable branch. The set can be accomplished by raising the input intensity beyond the switch-up threshold, whereas the reset operation can be effected by reducing the input intensity beyond switch-down intensity. So, the switch-up and -down intensities can serve as read and write bias pulse for the memory operation [20]. The memory holding width can be altered by changing the magnitude of the detuning parameter.

In the presence of second focusing (septimal) nonlinearity, the negative detuning regime shows the growth in the dormant stable states, whereas in the positive detuning regime the switch-down intensity decreases in addition to the shrinkage in the hysteresis loop as seen in Fig. 10(c). Operating at longer wavelengths has a marginal impact in the reduction of switch-up intensity, quite similar to those occurring at the shorter wavelengths in the cubic-quintic case with the only difference being the number of stable states above the dormant states is comparably larger and are desirable for multilevel signal processing applications. Although we present only a few applications here, the system's ability to retain its memory of the past state for longer period can be subjected to detailed investigation in the future to build new all-optical devices.

C. Impact of nonlinear parameters

The nonlinear parameter purely depends on the type of glass material used. From the application perspective, researchers are left with many materials offering a wide range of nonlinearities from very high to low values [20]. The nonlinearity plays a crucial role in deciding the number of stable states and the intensity required to switch between the stable branches. To illustrate this, we first consider a simple case with only cubic nonlinearity. The first bistable curve starts to emerge at $\gamma = 1.4$ in our numerical simulations for $g = 5$ and the intensity for up switching is 1.256 which further reduces to 1.099 with an increase in γ (1.6). Any further increase in the value of γ gives rise to multistable states as a consequence of increase in the effective feedback to the system as seen in Fig. 11(a). Earlier in the unbroken regime, we stated a thumb rule to reduce the switching intensity which demands the nonlinear coefficient to be high. From our simulations, we confirm that the rule holds good in the broken regime too.

With the addition of quintic nonlinearity to the above system, it admits multistable states even at lower input intensities as seen in Fig. 11(b). To comprehend the role of quintic nonlinearity, we numerically vary Γ at a fixed value of gain and loss coefficient ($g = 5$). At $\Gamma = 1$, when the input intensity is slowly varied from zero, there is a linear increase of output intensity below 1.479 above which it switches to the second stable state. The output intensity again starts to vary linearly in the second stable branch for values between 1.479 and 2.396. Above this intensity, the system switches to the third stable branch. If the intensity is decreased, the switch-down intensity required to swap from the third branch to the second is 1.582 and to switch back to its initial state, the input intensity must be reduced further to 0.6803. When Γ is increased further, the switching intensity between various stable branches tapers off and new stable states appear within the same input intensity ($P_0 = 2$). For instance, when $\Gamma = 1.5$ the switch-up intensity to switch between the first and second stable states is measured to be 1.093. The switch-up intensity reduces below unity when the system is operated at $\Gamma = 2$.

Finally, we present the effect of septimal nonlinearity in the presence of both cubic and quintic nonlinearities with simulation parameters as $g = 5$, $\gamma = 1.5$, $\Gamma = 1$ and septimal nonlinearity (σ) is varied. A straightforward evidence one can

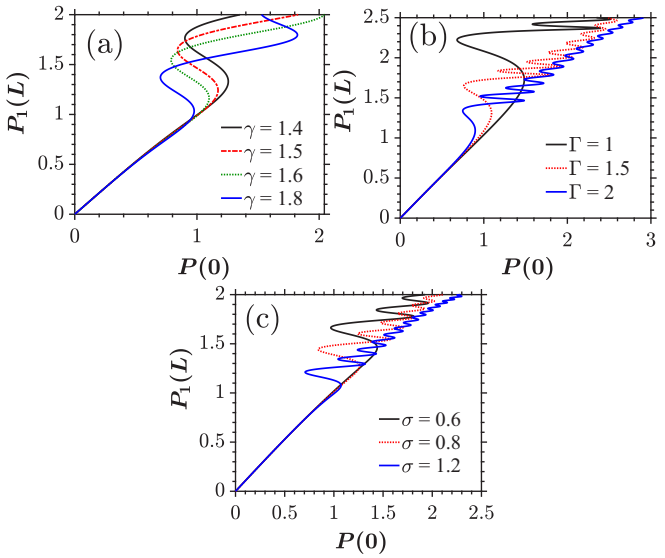

FIG. 11. Role of nonlinear coefficients on the optical bistability (multistability) of a broken $\mathcal{PT}$-symmetric FBG at $g = 5$ and $\delta = 0$. Here, the output and input powers are represented by $P_1(L)$ and $P(0)$, respectively. (a) Plotted for different values of cubic nonlinear coefficient (γ) at $\Gamma = \sigma = 0$. (b) Represents the simulated results for different values of quintic nonlinear coefficient (Γ) at $\gamma = 1.5$ and $\sigma = 0$. (c) Plotted for different values of septimal nonlinear coefficient (σ) at $\gamma = 1.5$ and $\Gamma = 1$.

get from Fig. 11(c) is that inclusion of the septimal nonlinearity cuts down the required intensity to switch between the stable states and the width of the hysteresis is further reduced when compared to the system with same simulation parameters in its absence. The septimal nonlinearity also boosts the number of stable states similar to the other nonlinear effects discussed already. When $\sigma = 0.8$, it supports more than five stable branches with each branch possessing a width narrower than the previous one. When $\sigma = 0.6$, a series of multistable states appear and the intensities to jump from the preceding state are 1.44 (1 to 2), 1.809 (2 to 3), and the respective switch-down intensities are given by 0.9697 and 1.433 as shown in Fig. 11(c). The width of the upper stable branches drastically reduces. But, with suitable adjustment in other device parameters, it is possible to increase the visibility of the upper stable states and hence such bistable states can lead to the efficient all-optical signal processing by controlling (output) light with (input) light. Also, a possible experimental realization of the kind of structure envisaged in this paper is to identify a suitable material (preferably chalcogenide glass) which can allow the fabrication of alternate regions of gain (actively doped by erbium) and loss (no dopant by considering the intrinsic loss or dopant with high absorption by chromium element) into it and thereby serving as a $\mathcal{PT}$-symmetric periodic structure.

V. EXISTENCE OF GAP SOLITONS

Soliton formation is a universal phenomenon that can occur in any nonlinear optical structures through a delicate interplay between the group-velocity dispersion and the nonlinearity of the structure. The former tends to disperse the energy of the propagating pulse, whereas the latter is supposed to counterbalance the effect caused by the former by concentrating the energy of the pulse [63]. Many types of solitons are reported theoretically and experimentally in the regular optical fibers which include dissipative [64], vector [65], polarization domain wall [66], dispersion managed, Raman, and paired solitons [63], as well as multisolitons [67], which rely on the above-mentioned phenomenon. Among them, gap solitons are a special type of solitons formed in the periodic structures which possess photonic band gap as a consequence of periodic variation in the linear dielectric constant. This periodic variation can often be engineered at ease [68] and, hence, gap solitons are well suited for applications such as optical buffering [69], optical delay lines [70], distributed feedback pulse generator [71], transmission filters [72], and logic gates [73].

The phenomenon of optical bistability in the feedback structures goes hand in hand with the formation of gap soliton [71]. To understand the dynamics of gap solitons, it is necessary to look back at the light transmission ($T = |\frac{u(L)}{u(0)}|^2$) characteristics of the device. In the distributed feedback periodic structures, the light propagation is portrayed by the existence of stop bands and pass bands. In a linear FBG, a wave is reflected if its wavelength falls within this forbidden band. Then again, a wave whose wavelength falls outside this stop band can traverse through the structure unhampered [52]. As pointed out by Winful *et al.* [71], the wave amplitude falls off exponentially along the propagation direction in this case. However, in the presence of nonlinearities, the light is totally transmitted for certain intensities due to the formation of *localized modes* or *spatial nonlinear resonances* within the stop band. These spatial resonances are coined as gap solitons simply for two reasons. First, they have the trademark shape of sech^2 solitons. Second, they reside within this photonic band gap. The formation of such gap solitons in the presence of Kerr effect in the conventional periodic structure has already been investigated by many authors [11,70,71]. Recently, the formation of gap solitons has been explored in $\mathcal{PT}$-symmetric periodic structures and some noteworthy properties were highlighted. In particular, it is shown that these phenomenological $\mathcal{PT}$-symmetric structures can support the interesting formation of dark-gap solitons [55]. In this section, our aim is to show that the gap solitons can persist even in the presence of higher-order nonlinearities in such $\mathcal{PT}$-symmetric systems. The first nonlinear resonance is observed at very low input intensities for a conventional FBG with $L = 1.5$, $k = 3$, $\gamma = 4$, $\Gamma = 1$, $\sigma = 2$, and $g = 0$ [see Fig. 12(a)]. The plot of forward field intensities against the propagation distance at the first peaks reveals that a bright-gap-soliton-like entity corresponding to the resonance value appears. We can observe that the difference between the forward and backward field intensity is marginal in Fig. 12(c). At sufficiently larger input intensities, a second-order-soliton-like entity is formed at the transmission resonance. The peak power of the forward field distribution curve is enhanced whereas the peak power of the backward field distribution is reduced at the successive transmission peaks as seen in Fig. 12(d). In both cases, the total power remains constant throughout the propagation length.

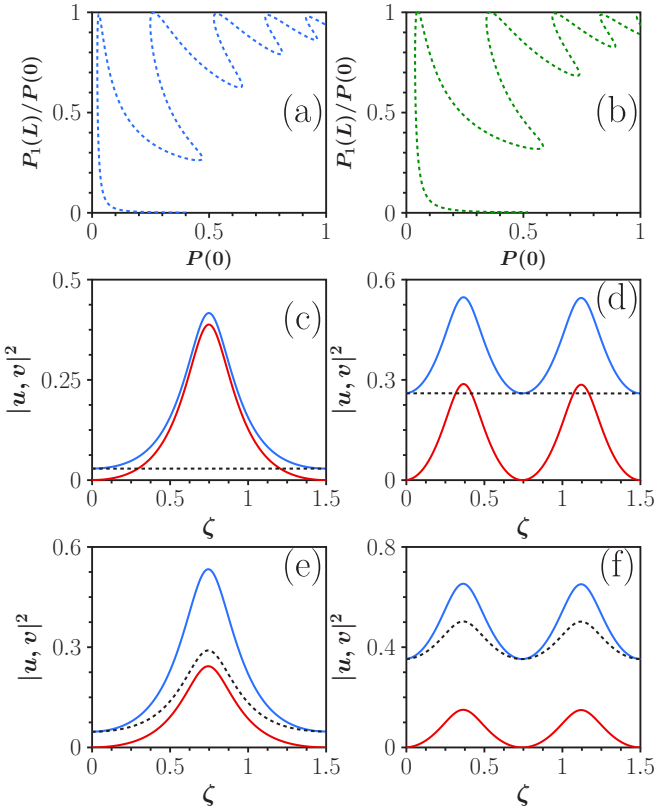

FIG. 12. Top panels (a) and (b) illustrate the transmission characteristics of conventional and $\mathcal{PT}$-symmetric FBGs, respectively. Center and bottom panels delineate the stationary gap soliton formation at the different resonance peaks for conventional and $\mathcal{PT}$-symmetric systems, respectively, when the parameters are kept as $L = 1.5$, $k = 3$, $g = 2$, $\delta = 1$, $\gamma = 4$, $\Gamma = 1$, and $\sigma = 2$. Here, the blue solid lined curves indicate the forward field and red lined curves refer to backward field intensities. The total field intensities ($|u|^2 - |v|^2$) are drawn by black dashed lines.

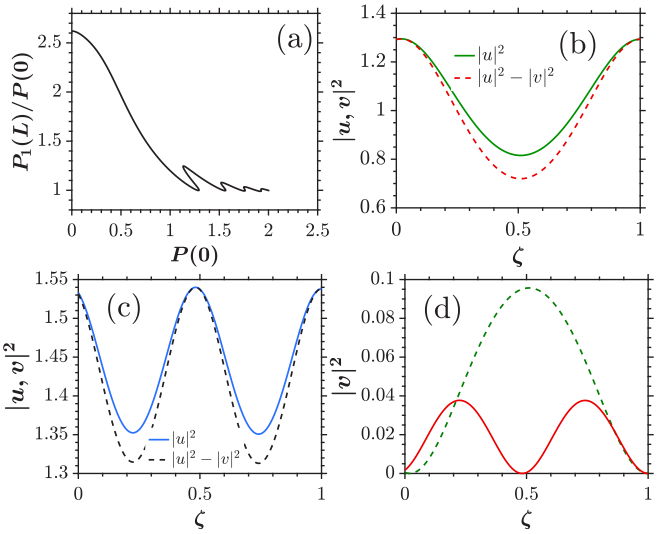

FIG. 13. Plots of (a) transmission (b) and (c) dark-gap-soliton formation in the broken $\mathcal{PT}$-symmetric regime and (d) illustrates the bright-gap-soliton-like entity in the broken regime. In (d) the dotted line corresponds to backward field intensity at the first transmission resonance and the solid line indicates the same at the second transmission resonance. The system parameters are chosen as $L = 1$, $\kappa = 2$, $g = 3$, $\delta = 0$ and the values of nonlinear parameters are taken to be $\gamma = \Gamma = \sigma = 1$.

When $\mathcal{PT}$ symmetry is included to the system ($g = 1$), these nonlinear resonances can still exist in Fig. 12(b). The plot also depicts that the $\mathcal{PT}$ symmetry plays a significant role in altering the peak intensities of these nonlinear resonances. The first and second transmission peaks occur at slightly larger input intensities when compared to the conventional case in Fig. 12(c). Similar to the conventional case, the value of the forward field peak is enhanced and the backward field peak is reduced at the second transmission peak as seen in Fig. 12(f). The plot of total intensity [see Figs. 12(e) and 12(f)] against the propagation distance also shows a bright-soliton-like entity unlike the conventional case. Motivated by the formation of unique gap soliton obtained in the unbroken regime, we next intend to examine whether these kinds of nonlinear resonances can occur in the broken regime too in the presence of higher-order nonlinearities. Numerical simulations turn out a surprising outcome of localized modes at the band gap which resembles a dark soliton in the broken regime as seen in Fig. 13. The $\mathcal{PT}$ symmetry dictates the value of the dip of the dark-soliton-like entity as in the case of forward field intensity distribution and total power distribution as seen in Figs. 13(b) and 13(c). On the other hand, one can observe that the simultaneous existence of bright-soliton-like entity in the plot of backward field distribution against the propagation distance [see Fig. 13(d)], which further can be regarded as the unique outcome of $\mathcal{PT}$ symmetry in such periodic structures.

VI. NONLINEAR REFLECTION SPECTRUM FOR CONSTANT PUMP POWER

In the previous sections, we elaborated the switching exhibited by the $\mathcal{PT}$-symmetric system under different conditions. But, in all the systems discussed previously, switching is achieved via optical bistability (multistability) under continuous variation in the pump power [P(0)]. We can also find that the FBG exhibits another type of switching mechanism in the presence of constant pump power [$P(0)$] as a function of detuning parameter (δ) in the literature in both linear [5] as well as nonlinear regimes [3,20]. These studies are restricted to only conventional FBGs without gain and loss. Hence, we are interested in studying this kind of switching behavior in the presence of $\mathcal{PT}$ symmetry. To do so, we fix $L = 0.5$, $k = 2$ and vary the other parameters for the unbroken $\mathcal{PT}$-symmetric regime, whereas we fix $L = 1$ and $k = 2$ for the broken $\mathcal{PT}$-symmetric regime.

A. Effect of variations in the nonlinearity in the unbroken $\mathcal{PT}$-symmetric regime

In the absence of any nonlinearity, the reflection spectrum is centered at $\delta = 0$. The spectrum is shifted toward longer wavelength when a cubic nonlinearity is added to the system. With further increase in the cubic nonlinearity parameter (γ), the spectrum is blueshifted [55]. Since quintic nonlinearity is a self-defocusing nonlinearity, the spectrum is shifted toward

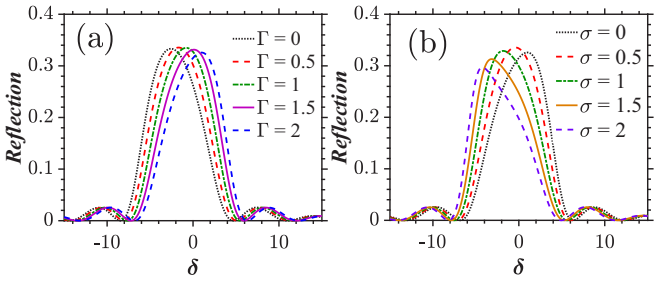

FIG. 14. Role of nonlinear coefficients on the reflection characteristics under constant pump power of an unbroken $\mathcal{PT}$-symmetric FBG at $g = 0.5$. (a) Represents the simulated results for different values of quintic nonlinear coefficient (Γ) at $\gamma = 2$ and $\sigma = 0$. (b) Plotted for different values of septimal nonlinear coefficient (σ) at $\gamma = \Gamma = 2$.

shorter wavelength with increase in Γ. In addition to shifting, the amount of light which is reflected by the system is reduced slightly with increase in Γ as seen in Fig. 14(a). The same kind of phenomenon is observed in the presence of an additional self-focusing nonlinearity (septimal) but the shifting of the spectrum is toward longer wavelength similar to cubic nonlinearity case [see Fig. 14(b)]. Thus, we can conclude that the shifting of the spectrum toward longer or shorter wavelength is dependent upon the nature of nonlinearities. Note that the effect of nonlinearity on the side lobes of the spectra (spectrum outside the band edges) is minimal.

B. Effect of variations in the gain or loss in the unbroken $\mathcal{PT}$-symmetric regime

In the absence of any $\mathcal{PT}$ symmetry and nonlinearities, the reflection is maximum around the Bragg wavelength. The wavelength at which the peak reflectivity occurs is varied by the presence of nonlinearities [55]. In Figs. 15(a) and 15(b) we can observe that the reflection peak is slightly off centered as a consequence of higher-order nonlinearity in the system. Any variation in the gain or loss does not shift the spectrum as in the case of nonlinearity. But, the actual effect of variation in the parameter g depends on the launching conditions. The band gap is more or less symmetric about the center wavelength in the presence of cubic nonlinearity

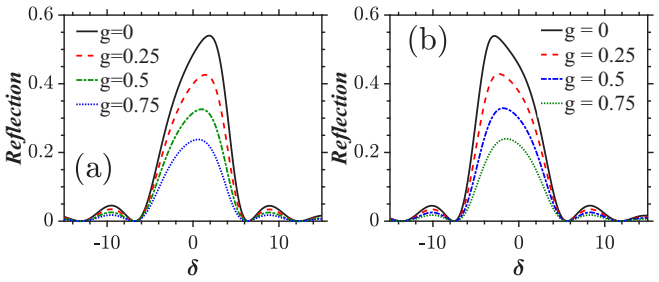

FIG. 15. Effect of variation in the gain-loss parameter (g) on the reflection characteristics under constant pump power of an unbroken $\mathcal{PT}$-symmetric FBG. (a) Represents the simulated results for different values of g in the presence of cubic-quintic nonlinearities ($\gamma = \Gamma = 2$, $\sigma = 0$). (b) Plotted for different values of g in the presence of cubic-quintic-septimal nonlinearities (σ) at $\gamma = \Gamma = 2$.

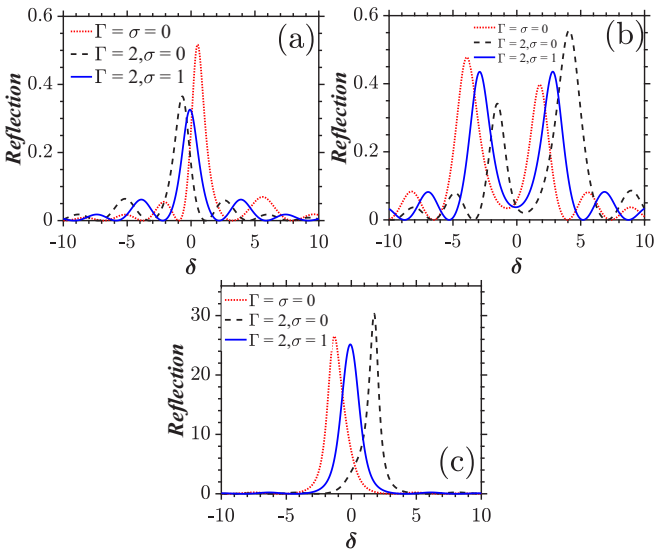

FIG. 16. Reflection characteristics under constant pump power of a broken $\mathcal{PT}$-symmetric FBG. (a)–(c) Plotted at $g = 3, 4, 5$, respectively. Throughout the figure the value of cubic nonlinear coefficient is set to $\gamma = 1$. The dotted lines (red) represent the cubic nonlinear regime ($\Gamma = \sigma = 0$). The dashed lines (black) indicate the quintic nonlinear regime ($\Gamma = 2, \sigma = 0$). The solid lines (blue) represent the septimal nonlinear regime ($\Gamma = 2, \sigma = 1$).

alone ($\gamma = 1$, $\Gamma = \sigma = 0$). For left incidence, the reflectivity is suppressed with increase in the gain or loss. When we look into the system with higher-order nonlinearities, the same effect persists. Thus, we can conclude that irrespective of the type of nonlinearity, the amount of light reflected is reduced by the gain-loss parameter g for the left incidence.

C. Unique spectra in the broken $\mathcal{PT}$-symmetric regime

In the unbroken $\mathcal{PT}$-symmetric regime, the reflection characteristics are found to be more or less flat within the stop band. But, in the broken $\mathcal{PT}$-symmetric regime, the peak of the reflection occurs at a single wavelength instead of the entire stop band as in the case of Fig. 16(a) which is simulated at $g = 3$. Any additional nonlinearities in the form of quintic nonlinearity or septimal nonlinearity shift the peak of the reflection toward longer wavelengths. When $g = 4$, the reflection spectrum begins to divide into two and thus we can observe two separate peaks on either side of $\delta = 0$ [see Fig. 16(b)]. The first peak corresponds to negative detuning values of δ and the second peak corresponds to positive detuning values. The reflected power is not the same in these peaks. More power is accumulated at the peak lying on the shorter wavelength side compared to its counterpart. But, closer to $\delta = 0$ the reflection is minimum. This kind of behavior is unique because in both conventional FBG [5] and unbroken $\mathcal{PT}$ symmetry the reflection is maximum within the stop band and at the band edges the reflection is minimum. Even more interestingly, when $g = 5$ the reflection is completely prohibited in the side lobes unlike the other cases and the reflection is maximum at a single wavelength rather than band of wavelengths. Otherwise, this can be called as a lasinglike behavior, with large reflected intensity at the lasing

wavelength. Moreover, the presence of quintic nonlinearity redshifts the spectrum instead of a blueshift in both Figs. 16(b) and 16(c) unlike the previous cases.

VII. CONCLUSION

In this paper we have presented a detailed study on the optical bistability and multistability phenomena as well as nonlinear reflection spectra in a highly nonlinear fiber Bragg grating influenced by $\mathcal{PT}$-symmetry conditions. We have reported unique behaviors such as ramplike and steplike stable states in the broken $\mathcal{PT}$-symmetric regime which were previously believed to exist only in complex optical structures involving plasmons, graphene, etc. We affirm that these states are feasible in a simple FBG device with minimal effort by having a balance between gain and loss of the system. We have also found alternative optical bistabilities in the broken $\mathcal{PT}$-symmetric regime which can pave a new way to the low-power switches via reversal of the direction of light incidence. This confirms that FBG offers a fertile ground to unearth unique nonlinear functionalities in the $\mathcal{PT}$-symmetry broken regime in addition to the unbroken regime. We have also depicted the existence of both dark- and bright-soliton-like entities at the transmission resonances. We would like to leave an end note that all the numerical experiments presented here deserve further investigations through practical observations, and this could open the door for new generation of multifunctional optical devices including optical switches and memories. To be regarded as the next-generation multifunctional devices, any system must address some of the important criteria like size miniature, reduction in cost, low-power consumption, design flexibility, and so on, and our ramifications rely on the last two aspects, i.e., optical switches with low switching intensities and flexibility to set up the desired application simply by tuning one of the control parameters. In addition, our system can play a key role to set up a new generation of all-optical regenerators employing PAM scheme in the near future as our system admits a large number of stable states with low switching intensities, which is an ideal requirement for any all-optical systems.

ACKNOWLEDGMENTS

S.V.R. is indebted to the financial assistantship provided by Anna University through Anna Centenary Research Fellowship (Grant No. CFR/ACRF-2018/AR1/24). A.G. thanks the Department of Science and Technology, Ministry of Science and Technology (DST) and Science and Engineering Research Board (SERB), Government of India, for providing a National Postdoctoral Fellowship (Grant No. PDF/2016/002933). M.L. is supported by DST-SERB through a Distinguished Fellowship (Grant No. SB/DF/04/2017). A.G. and M.L. also thank Council of Scientific and Industrial Research (Grant No. 03/1331/15/EMR-II).

[1] S. Jenson, The nonlinear coherent coupler, IEEE J. Quantum Electron. **18**, 1580 (1982).

[2] A. Govindaraji, A. Mahalingam, and A. Uthayakumar, Numerical investigation of dark soliton switching in asymmetric nonlinear fiber couplers, Appl. Phys. B **120**, 341 (2015).

[3] Z. Zang and Y. Zhang, Analysis of optical switching in a yb^{3+}-doped fiber Bragg grating by using self-phase modulation and cross-phase modulation, Appl. Opt. **51**, 3424 (2012).

[4] P. Sethi and S. Roy, All-optical ultrafast switching in 2×2 silicon microring resonators and its application to reconfigurable demux/mux and reversible logic gates, J. Light. Technol. **32**, 2173 (2014).

[5] T. Erdogan, Fiber grating spectra, J. Light. Technol. **15**, 1277 (1997).

[6] R. Ramaswami, K. Sivarajan, and G. Sasaki, *Optical Networks: A Practical Perspective* (Morgan Kaufmann, Amsterdam, 2009).

[7] K. O. Hill and G. Meltz, Fiber Bragg grating technology fundamentals and overview, J. Light. Technol. **15**, 1263 (1997).

[8] S. Radic, N. George, and G. P. Agrawal, Theory of low-threshold optical switching in nonlinear phase-shifted periodic structures, J. Opt. Soc. Am. B **12**, 671 (1995).

[9] Y. D. Jeong, J. S. Cho, Y. H. Won, H. J. Lee, and H. Yoo, All-optical flip-flop based on the bistability of injection locked Fabry–Pérot laser diode, Opt. Express **14**, 4058 (2006).

[10] Q. Li, H. Yuan, and X. Tang, Bistability and all-optical flip–flop with active microring resonator, Appl. Opt. **53**, 3049 (2014).

[11] N. M. Litchinitser, I. R. Gabitov, and A. I. Maimistov, Optical Bistability in a Nonlinear Optical Coupler with a Negative Index Channel, Phys. Rev. Lett. **99**, 113902 (2007).

[12] A. Govindarajan, B. A. Malomed, and M. Lakshmanan, Nonlinear anti-directional couplers with gain and loss, Opt. Lett. **44**, 4650 (2019).

[13] Y. Yosia, S. Ping, and L. Chao, Bistability threshold inside hysteresis loop of nonlinear fiber Bragg gratings, Opt. Express **13**, 5127 (2005).

[14] E. Yousefi, M. Hatami, and A. T. Jahromi, All-optical ternary signal processing using uniform nonlinear chalcogenide fiber Bragg gratings, J. Opt. Soc. Am. B **32**, 1471 (2015).

[15] H. Gibbs, *Optical Bistability: Controlling Light with Light* (Elsevier, Amsterdam, 2012).

[16] H. G. Winful, J. Marburger, and E. Garmire, Theory of bistability in nonlinear distributed feedback structures, Appl. Phys. Lett. **35**, 379 (1979).

[17] C.-X. Shi, Optical bistability in reflective fiber gratings, IEEE J. Quantum Electron. **31**, 2037 (1995).

[18] J. Harbold, F. Ilday, F. Wise, J. Sanghera, V. Nguyen, L. Shaw, and I. Aggarwal, Highly nonlinear As–S–Se glasses for all-optical switching, Opt. Lett. **27**, 119 (2002).

[19] Y.-F. Chen, K. Beckwitt, F. W. Wise, B. G. Aitken, J. S. Sanghera, and I. D. Aggarwal, Measurement of fifth-and seventh-order nonlinearities of glasses, J. Opt. Soc. Am. B **23**, 347 (2006).

[20] M. Karimi, M. Lafouti, A. A. Amidiyan, and J. Sabbaghzadeh, All-optical flip-flop based on nonlinear effects in fiber Bragg gratings, Appl. Opt. **51**, 21 (2012).

[21] K. Porsezian, K. Senthilnathan, and S. Devipriya, Modulational instability in fiber Bragg grating with non-kerr nonlinearity, IEEE J. Quantum Electron. **41**, 789 (2005).

[22] H. Triki, K. Porsezian, A. Choudhuri, and P. T. Dinda, Chirped solitary pulses for a nonic nonlinear Schrödinger equation on a continuous-wave background, Phys. Rev. A **93**, 063810 (2016).

[23] H. Triki, K. Porsezian, P. T. Dinda, and P. Grelu, Dark spatial solitary waves in a cubic-quintic-septimal nonlinear medium, Phys. Rev. A **95**, 023837 (2017).

[24] J. Atai and B. A. Malomed, Families of Bragg-grating solitons in a cubic-quintic medium, Phys. Lett. A **155**, 247 (2001).

[25] A. S. Reyna, B. A. Malomed, and C. B. de Araújo, Stability conditions for one-dimensional optical solitons in cubic-quintic-septimal media, Phys. Rev. A **92**, 033810 (2015).

[26] N. Broderick, D. Taverner, and D. J. Richardson, Nonlinear switching in fibre Bragg gratings, Opt. Express **3**, 447 (1998).

[27] Y. Yosia and S. Ping, Double optical bistability and its application in nonlinear chalcogenide-fiber Bragg gratings, Phys. B (Amsterdam) **394**, 293 (2007).

[28] S. Ping, L. Chao *et al.*, Nonlinear switching and pulse propagation in phase-shifted cubic quintic grating, IEEE Photon. Technol. Lett. **17**, 2670 (2005).

[29] A. Lupu, H. Benisty, and A. Degiron, Switching using $\mathcal{PT}$-symmetry in plasmonic systems: Positive role of the losses, Opt. Express **21**, 21651 (2013).

[30] T. Kottos, Optical physics: Broken symmetry makes light work, Nat. Phys. **6**, 166 (2010).

[31] R. El-Ganainy, K. Makris, D. Christodoulides, and Z. H. Musslimani, Theory of coupled optical $\mathcal{PT}$-symmetric structures, Opt. Lett. **32**, 2632 (2007).

[32] A. Govindarajan, A. K. Sarma, and M. Lakshmanan, Tailoring $\mathcal{PT}$-symmetric soliton switch, Opt. Lett. **44**, 663 (2019).

[33] S. Karthiga, V. K. Chandrasekar, M. Senthilvelan, and M. Lakshmanan, Controlling of blow-up responses by nonlinear $\mathcal{PT}$-symmetric coupling, Phys. Rev. A **95**, 033829 (2017).

[34] L. Feng, Y.-L. Xu, W. S. Fegadolli, M.-H. Lu, J. E. Oliveira, V. R. Almeida, Y.-F. Chen, and A. Scherer, Experimental demonstration of a unidirectional reflectionless parity-time metamaterial at optical frequencies, Nat. Mater. **12**, 108 (2013).

[35] S. Longhi and L. Feng, $\mathcal{PT}$-symmetric microring laser-absorber, Opt. Lett. **39**, 5026 (2014).

[36] C. Huang, R. Zhang, J. Han, J. Zheng, and J. Xu, Type-ii perfect absorption and amplification modes with controllable bandwidth in combined $\mathcal{PT}$-symmetric and conventional Bragg-grating structures, Phys. Rev. A **89**, 023842 (2014).

[37] S. Phang, A. Vukovic, H. Susanto, T. M. Benson, and P. Sewell, Ultrafast optical switching using parity–time symmetric Bragg gratings, J. Opt. Soc. Am. B **30**, 2984 (2013).

[38] L. Feng, Z. J. Wong, R.-M. Ma, Y. Wang, and X. Zhang, Single-mode laser by parity-time symmetry breaking, Science **346**, 972 (2014).

[39] S. Longhi, $\mathcal{PT}$-symmetric laser absorber, Phys. Rev. A **82**, 031801(R) (2010).

[40] C. M. Bender and S. Boettcher, Real Spectra in Non-Hermitian Hamiltonians having $\mathcal{PT}$- Symmetry, Phys. Rev. Lett. **80**, 5243 (1998).

[41] Z. Lin, H. Ramezani, T. Eichelkraut, T. Kottos, H. Cao, and D. N. Christodoulides, Unidirectional Invisibility Induced by $\mathcal{PT}$-Symmetric Periodic Structures, Phys. Rev. Lett. **106**, 213901 (2011).

[42] L. Razzari and R. Morandotti, Optics: Gain and loss mixed in the same cauldron, Nature (London) **488**, 163 (2012).

[43] C. E. Rüter, K. G. Makris, R. El-Ganainy, D. N. Christodoulides, M. Segev, and D. Kip, Observation of parity-time symmetry in optics, Nat. Phys. **6**, 192 (2010).

[44] B. Baum, H. Alaeian, and J. Dionne, A parity-time symmetric coherent plasmonic absorber-amplifier, J. Appl. Phys **117**, 063106 (2015).

[45] L. Chang, X. Jiang, S. Hua, C. Yang, J. Wen, L. Jiang, G. Li, G. Wang, and M. Xiao, Parity-time symmetry and variable optical isolation in active-passive-coupled microresonators, Nat. Photon. **8**, 524 (2014).

[46] S. Phang, A. Vukovic, T. M. Benson, H. Susanto, and P. Sewell, A versatile all-optical parity-time signal processing device using a Bragg grating induced using positive and negative Kerr-nonlinearity, Opt. Quantum Electron. **47**, 37 (2015).

[47] S. Phang, A. Vukovic, H. Susanto, T. M. Benson, and P. Sewell, Impact of dispersive and saturable gain/loss on bistability of nonlinear parity–time Bragg gratings, Opt. Lett. **39**, 2603 (2014).

[48] J. Liu, X.-T. Xie, C.-J. Shan, T.-K. Liu, R.-K. Lee, and Y. Wu, Optical bistability in nonlinear periodical structures with $\mathcal{PT}$-symmetric potential, Laser Phys. **25**, 015102 (2015).

[49] A. K. Sarma, Modulation instability in nonlinear complex parity-time symmetric periodic structures, J. Opt. Soc. Am. B **31**, 1861 (2014).

[50] M.-A. Miri, A. B. Aceves, T. Kottos, V. Kovanis, and D. N. Christodoulides, Bragg solitons in nonlinear $\mathcal{PT}$-symmetric periodic potentials, Phys. Rev. A **86**, 033801 (2012).

[51] M. Komissarova, V. Marchenko, and P. Y. Shestakov, $\mathcal{PT}$-symmetric periodic structures with the modulation of the Kerr nonlinearity, Phys. Rev. E **99**, 042205 (2019).

[52] G. Agrawal, *Applications of Nonlinear Fiber Optics* (Elsevier, Amsterdam, 2001).

[53] X.-Y. Zhou, B.-J. Wu, Q.-Y. Wan, F. Wen, and K. Qiu, Optical multi-stability in fiber Bragg gratings with application to all-optical regeneration of multi-level pulse-amplitude-modulation signals, in *Asia Communications and Photonics Conference* (Optical Society of America, Washington, DC, 2014), pp. ATh3A–119.

[54] S. Radic, N. George, and G. P. Agrawal, Optical switching in λ/4-shifted nonlinear periodic structures, Opt. Lett. **19**, 1789 (1994).

[55] A. Govindarajan and M. Lakshmanan (unpublished).

[56] N. Daneshfar and T. Naseri, Switching between optical bistability and multistability in plasmonic multilayer nanoparticles, J. Appl. Phys. **121**, 023111 (2017).

[57] X. Dai, L. Jiang, and Y. Xiang, Low threshold optical bistability at terahertz frequencies with graphene surface plasmons, Sci. Rep. **5**, 12271 (2015).

[58] M. A. Sharif, M. M. Ara, B. Ghafary, S. Salmani, and S. Mohajer, Experimental observation of low threshold optical bistability in exfoliated graphene with low oxidation degree, Opt. Mater. **53**, 80 (2016).

[59] T. Naseri, N. Daneshfar, M. Moradi-Dangi, and F. Eynipour-Malaee, Terahertz optical bistability of graphene-coated cylindrical core–shell nanoparticles, J. Theor. Appl. Phys. **12**, 257 (2018).

[60] I. D. Rukhlenko, M. Premaratne, and G. P. Agrawal, Analytical study of optical bistability in silicon-waveguide resonators, Opt. Express **17**, 22124 (2009).

[61] T. Naseri and N. Daneshfar, Optical bistability of a plexcitonic system consisting of a quantum dot near a metallic nanorod, J. Theor. Appl. Phys. **12**, 183 (2018).

[62] N. Ogasawara and R. Ito, Static and dynamic properties of nonlinear semiconductor laser amplifiers, Jpn. J. Appl. Phys. **25**, L739 (1986).

[63] A. Hasegawa and Y. Kodama, *Solitons in Optical Communications*, No. 7 (Clarendon Press, Oxford, 1995).

[64] L. Zhao, D. Tang, X. Wu, and H. Zhang, Dissipative soliton generation in yb-fiber laser with an invisible intracavity bandpass filter, Opt. Lett. **35**, 2756 (2010).

[65] D. Tang, H. Zhang, L. Zhao, and X. Wu, Observation of High-Order Polarization-Locked Vector Solitons in a Fiber Laser, Phys. Rev. Lett. **101**, 153904 (2008).

[66] H. Zhang, D. Y. Tang, L. Zhao, and X. Wu, Observation of polarization domain wall solitons in weakly birefringent cavity fiber lasers, Phys. Rev. B **80**, 052302 (2009).

[67] Y. Chen, M. Wu, P. Tang, S. Chen, J. Du, G. Jiang, Y. Li, C. Zhao, H. Zhang, and S. Wen, The formation of various multi-soliton patterns and noise-like pulse in a fiber laser passively mode-locked by a topological insulator based saturable absorber, Laser Phys. Lett. **11**, 055101 (2014).

[68] H. G. Winful and V. Perlin, Raman Gap Solitons, Phys. Rev. Lett. **84**, 3586 (2000).

[69] J. T. Mok, C. M. De Sterke, I. C. Littler, and B. J. Eggleton, Dispersionless slow light using gap solitons, Nat. Phys. **2**, 775 (2006).

[70] G. D'Aguanno, N. Mattiucci, M. Scalora, and M. J. Bloemer, Bright and Dark Gap Solitons in a Negative Index Fabry–Pérot Etalon, Phys. Rev. Lett. **93**, 213902 (2004).

[71] H. G. Winful, R. Zamir, and S. Feldman, Modulational instability in nonlinear periodic structures: Implications for "gap solitons", Appl. Phys. Lett. **58**, 1001 (1991).

[72] A. Kozhekin and G. Kurizki, Self-Induced Transparency in Bragg Reflectors: Gap Solitons Near Absorption Resonances, Phys. Rev. Lett. **74**, 5020 (1995).

[73] D. Taverner, N. Broderick, D. Richardson, M. Ibsen, and R. Laming, All-optical and gate based on coupled gap-soliton formation in a fiber bragg grating, Opt. Lett. **23**, 259 (1998).